J. Fluid Mech. (1985), *vol.* 154, *pp.* 509–529
Printed in Great Britain

Scattering of acoustic waves into Tollmien–Schlichting waves by small streamwise variations in surface geometry

By M. E. GOLDSTEIN
National Aeronautics and Space Administration, Lewis Research Center, Cleveland, Ohio 44135

(Received 7 August 1984)

By using the triple-deck scaling of Stewartson (1969) and Messiter (1970) we show that small but relatively sudden surface geometry variations that produce only very weak static pressure variations can nevertheless produce strong, i.e. $O(1)$, coupling between an externally imposed acoustic disturbance and a spatially growing Tollmien– Schlichting wave. The analysis provides a qualitative explanation of the Leehey & Shapiro (1979) boundary-layer receptivity measurements and is in good quantitative agreement with the Aizin & Polyakov (1979) experiment. It may also explain why small 'trip wires' can promote early transition.

1. Introduction

It is now clear that transition to turbulence in boundary layers frequently begins with the excitation of Tollmien–Schlichting waves by very weak freestream disturbances and that the transition Reynolds number is strongly affected by the nature and strength of these disturbances. A number of investigators have attempted to study this phenomenon by minimizing the natural disturbances in their experiments and imposing controlled (i.e. known) disturbances of some particular type. Acoustic disturbances were found to be especially effective in this role (primarily because of their large spanwise coherence) and Shapiro (1977) (see also Leehey & Shapiro 1979) carried out a very interesting experiment in which a disturbance of this type was imposed on a flat plate boundary layer without producing any significant vibration of the plate. Shapiro's Mach number was quite low and his imposed disturbance was a nearly plane wave propagating in the mean-flow direction, so that it acted, for practical purposes, like a uniform pulsation of the entire stream.

He found (1) that the resulting Tollmien–Schlichting wave amplitude increased linearly with that of the imposed disturbance – indicating that the former was generated by a strictly linear process – and (2) that the maximum Tollmien–Schlichting wave amplitude at the lower branch of the neutral-stability curve was, in fact, nearly equal to that of the imposed disturbance; which is to say that the observed 'coupling coefficient' was very nearly equal to one.

The effect of a uniformly pulsating stream on the flow over an *infinitely thin* flat plate was studied numerically by Murdock (1980) and analytically by Goldstein (1983*a*, *b*) and by Goldstein, Sockol & Sanz (1983). They found that the resulting Tollmien–Schlichting waves were several orders of magnitude smaller at the lower branch of the neutral-stability curve than those measured by Shapiro (1977).

Goldstein's (1983*a*, *b*) analysis shows (1) that the Tollmien–Schlichting waves are generated near the leading edge, where non-parallel-flow effects become important,

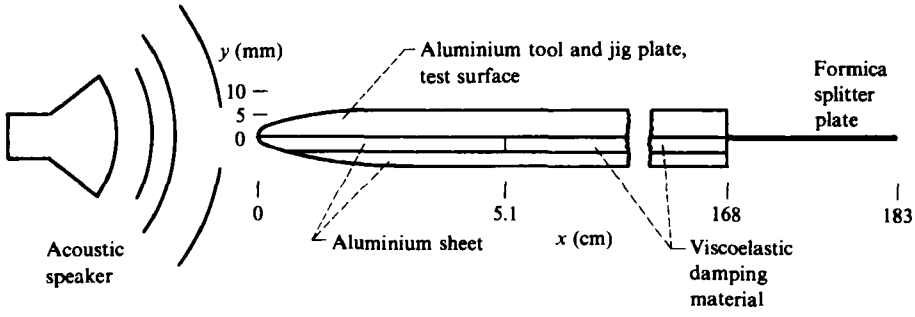

FIGURE 1. Shapiro's (1977) plate.

and (2) that these waves then undergo considerable decay before reaching the neutral-stability point, where they can start to grow. The decay process is related to the reduction of the (effectively infinite) wavelength of the free-stream disturbance that must take place before it can turn into a very short wavelength Tollmien–Schlichting wave. Goldstein (1983*a*,*b*) also finds that the coupling coefficient itself is quite weak in this case.

However, Shapiro's (1977) plate was certainly not infinitely thin, and he, in fact, detected weak but relatively rapid streamwise variations in static pressure, which presumably resulted from streamwise variations in plate thickness. The purpose of the present paper is to show that even the very small streamwise variations in surface geometry that cause such weak static pressure variations can produce a large coupling between Tollmien–Schlichting waves and the imposed disturbance when these variations are sufficiently rapid, i.e. when they occur on the scale of a Tollmien–Schlichting wavelength. The variations in surface geometry are then able to 'scatter' very long-wavelength acoustic disturbances into the much shorter-wavelength Tollmien–Schlichting waves.

The required variation in surface geometry may have occurred at the junction of the 'nose' and 'flat-plate' regions of Shapiro's (1977) plate, shown here as figure 1. But, since this point was upstream of the neutral-stability point in his experiment, the Tollmien–Schlichting waves generated at the former point would still have had to undergo a certain amount of decay before they reached the latter, as was the case for the infinitely thin flat plate studied by Murdock (1980), Goldstein (1983*a*,*b*) and Goldstein *et al.* (1983). However, the present mechanism produces strong-enough coupling and small-enough decay ($< 10^{-1}$) to account for Shapiro's observed unit amplitude ratio at the neutral-stability point. Large leading-edge curvature would produce Tollmien–Schlichting waves that are negligably small because they would have to undergo much more decay than those generated at the junction.

In order to reduce the problem to its simplest terms we consider a two-dimensional incompressible flow over a body with a small region of relatively large surface curvature (such as Shapiro's flat plate shown in figure 1). The upstream mean flow is assumed to be uniform, and we suppose that the unsteadiness is due to a small-amplitude time-harmonic pulsation of that flow.

Since the mean boundary-layer flow, and consequently the Tollmien–Schlichting waves that ride on that flow, can only be defined mathematically in the infinite-Reynolds-number limit, we suppose that the length Reynolds number R is large and carry out the analysis as a systematic asymptotic expansion in inverse powers of this quantity. We suppose that the streamwise extent of the large-curvature region is $O(R^{-\frac{1}{8}})$ and that the mean flow is turned through an angle $O(R^{-\frac{1}{4}})$ across this region.

The corresponding steady flow was studied by Stewartson (1970, 1971), and was found to possess the well-known 'triple-deck' structure of Stewartson (1969) and Messiter (1970). Stewartson showed that the resulting static-pressure variations were also $O(R^{-\frac{1}{4}})$.

The unsteady flow of the present analysis can be treated as a linear perturbation of Stewartson's (1970, 1971) solution, and therefore also possesses a 'triple-deck' structure. We suppose that the dimensionless frequency (i.e. Strouhal number) of the imposed disturbance is $O(R^{\frac{1}{4}})$, corresponding to the Tollmien–Schlichting wave frequency at the lower branch of the neutral-stability curve (Smith 1979; Goldstein 1983). Smith (1979) showed that Tollmien–Schlichting waves have a 'triple-deck' structure at the lower branch of the neutral-stability curve in the infinite-Reynolds-number limit, and Goldstein (1983*a*, *b*) showed that they also have this structure everywhere upstream of this curve. It is therefore natural that these waves should appear in the present analysis. We show that they occur just downstream of the region of large curvature, which we refer to as the interaction region, and that their amplitude is of the same order as that of the imposed disturbance (i.e. the coupling coefficient is of order one), which is rather remarkable, since the disturbance to the mean flow (as measured, say, by the mean-pressure variations) is so small ($O(R^{-\frac{1}{4}})$).

In §5 we explain how such small mean-flow variations are able to have such a large effect on the unsteady flow. We next show that the predicted static-pressure variations are quite compatible with measurements made by Shapiro (1977) during the course of his experiment. The theory is then compared with Goldstein's (1983*a*, *b*) infinitely thin flat-plate analysis and we explain why the coupling is so much stronger in the present case. Finally, the predictions of the present theory are shown to be consistent with the Tollmien–Schlichting wave amplitudes observed by Shapiro (1977).

Smith (1973) showed that Stewartson's (1970) analysis also applies to the flow over small humps on otherwise flat walls. The present study therefore applies to this case, and may consequently provide an explanation of how very small trip wires, and perhaps roughness elements, promote early transition.

Aizin & Polyakov (1979) conducted a relevant experiment wherein the Tollmien–Schlichting wave was generated by an upstream-propagating acoustic wave interacting with a thin Mylar strip. In §5.3 we show that the present theory is in excellent quantitative agreement with their data.

Section 5.4 explains how the theory can be applied to any type of imposed disturbance whose spatial scale is large compared with the Tollmien–Schlichting wavelength. Finally, §5.5 shows that the results of the present study remain valid over the entire range of unstable frequencies rather than over the restricted range near the lower branch of the neutral curve implied by the original scaling.

Nishioka & Morkovin (1985) recently imposed a very small-scale unsteady pressure gradient directly on a flat-plate boundary layer, so that the imposed disturbance and Tollmien–Schlichting wavelengths were compatible in their case. Their paper contains a qualitative description of the coupling process and provides a number of useful references to other experiments related to the present work.

2. Formulation

In order to fix ideas, we consider a two-dimensional incompressible flow of density ρ and kinetic viscosity ν over a relatively thin two-dimensional body having a small region of large surface curvature κ^*, as shown schematically in figure 2. The net turning of the flow across this region is assumed to be small in a sense to be prescribed

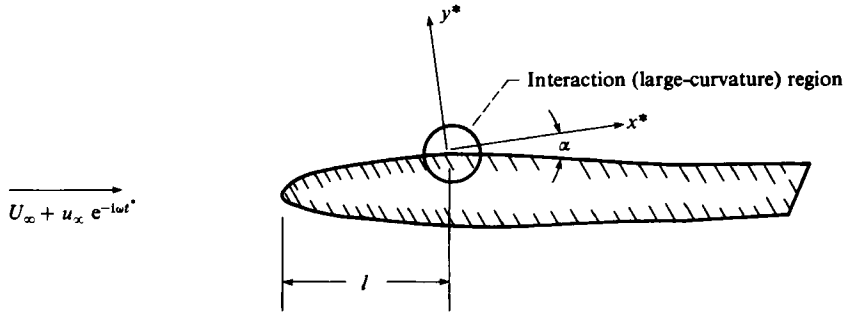

FIGURE 2. Flow configuration.

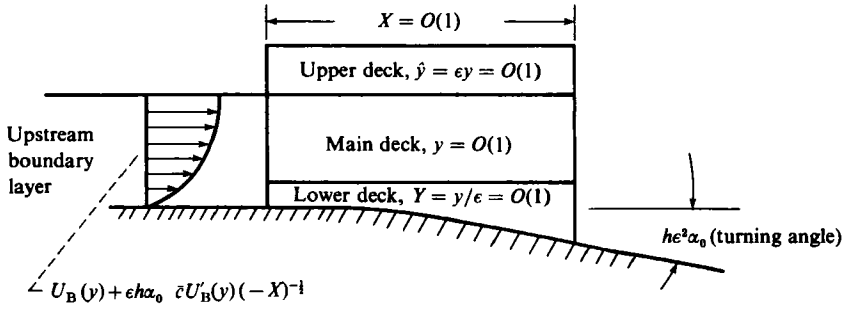

FIGURE 3. Structure of the interaction region.

more precisely below. The upstream motion consists of a uniform flow with velocity U_∞ plus a small harmonic perturbation of frequency ω and constant amplitude $u_\infty \ll U_\infty$, so that the unsteady motion can be treated as a linear perturbation of the steady flow corresponding to U_∞.

We introduce a Cartesian coordinate system $\{x^*, y^*\}$, with x^* tangent to the body surface just upstream of the large-curvature region as indicated in figure 2. The steady velocity $\{U_0, V_0\}$ and pressure P_0 are assumed to be normalized by U_∞ and ρU_∞^2 respectively, while the unsteady velocity perturbation $\{u, v\}$ and pressure perturbation p are assumed to be normalized by u_∞ and $\rho u_\infty U_\infty$ respectively.

As indicated in §1, the Reynolds number $R = U_\infty l/\nu$ based on the distance l between the leading edge and the region of large curvature is assumed to be large, and the net turning angle α across this region (see figure 2) and its curvature κ^* are assumed to be $O(\epsilon^2)$ and $O(l^{-1}\epsilon^{-1})$ respectively, where

$$\epsilon \equiv R^{-\frac{1}{8}}. \tag{2.1}$$

Then the viscous effects will, to lowest order, be confined to a narrow boundary layer of thickness ϵ^4 on the surface of the body, and the flow in the vicinity of the large-curvature region will be unseparated and have the 'triple-deck' structure of Stewartson (1969) and Messiter (1970), as indicated in figure 3. In fact, Stewartson (1970) has already analysed the steady flow in this region, and we treat the unsteady flow as a small perturbation about his solution. The latter flow bears some resemblance to the Brown & Daniels (1975) solution for unsteady trailing-edge flow, but differs from it in a number of important respects (e.g. the boundary conditions are different). The present work is also unique in combining such an unsteady solution

with classical boundary-layer stability theory and Stewartson's (1970) steady analysis for a change in wall slope. The work of Hall & Smith (1982) is also relevant to the present study.

Following Stewartson (1970), we introduce the scaled coordinates

$$X = \frac{x^*}{l\epsilon^3}, \quad y = \frac{y^*}{l\epsilon^4}. \tag{2.2}$$

Then the large-curvature portion of the body surface can be described by an equation of the form

$$y = \epsilon h F(X), \tag{2.3}$$

where $$F(X) \to 0, -\alpha_0 X \quad \text{as} \quad X \to -\infty, +\infty,$$

the scaled turning angle

$$\alpha_0 = \alpha/h\epsilon^2 \tag{2.4}$$

is assumed to be $O(1)$ as $\epsilon \to 0$, and h is a parameter introduced for later convenience.

2.1. *The steady flow*

The relevant portions of Stewartson's (1970) analysis are summarized in this subsection. He showed that the flow in the main deck, where $y = O(1)$, behaves like

$$U_0 \to U_B(y) + \epsilon h \alpha_0 \bar{c} U_B'(y) (-X)^{-\frac{1}{2}} \quad \text{as } X \to -\infty, \tag{2.5}$$

where $\bar{c}$ is a constant, $U_B(y)$ is the boundary-layer velocity profile just upstream of the 'triple deck' and the prime denotes differentiation with respect to the indicated argument. Since the body is assumed to be thin, we can take U_B to be the Blasius profile and assume that $U_B \to 1$ as $y \to \infty$.

Stewartson (1970) showed that the steady flow within the main deck itself has the structure

$$U_0 = U_B(y) + \epsilon A(X) U_B'(y) + O(\epsilon^2), \tag{2.6}$$

$$V_0 = -\epsilon^2 A'(X) U_B(y) + O(\epsilon^3), \tag{2.7}$$

$$P_0 = \epsilon^2 \ln \epsilon \frac{3\alpha_0 h}{\pi} + \epsilon^2 P(X) + O(\epsilon^3), \tag{2.8}$$

where A and P are related, via the upper-deck solution, by the Cauchy integral

$$A''(X) = \frac{1}{\pi} \int\!\!\!\!\!\!- _{-\infty}^{\infty} \frac{P'(\tilde{X})}{\tilde{X} - X} \, \mathrm{d}\tilde{X}, \tag{2.9}$$

and the slash indicates that the Cauchy principal value of the integral is to be taken.

The steady flow in the lower deck, where

$$Y \equiv y/\epsilon \tag{2.10}$$

is $O(1)$, has the structure

$$\left.\begin{aligned} U_0 &= \epsilon U(X, Y) + O(\epsilon^2), \\ V_0 &= \epsilon^3 V(X, Y) + O(\epsilon^4), \\ P_0 &= \epsilon^2 P(X) + O(\epsilon^3), \end{aligned}\right\} \tag{2.11}$$

where the scaled variables U, V and P are determined by the boundary-layer equations

$$UU_X + VU_Y = -P'(X) + U_{YY}, \tag{2.12}$$

$$U_X + V_Y = 0, \tag{2.13}$$

subject to the boundary conditions

$$U = V = 0, \quad Y = hF(X) \quad \text{for } -\infty < X < \infty, \tag{2.14}$$

$$U \to \lambda Y \quad \text{as } X \to -\infty, \tag{2.15}$$

$$U \to \lambda[Y + A(X)] \quad \text{as } Y \to +\infty, \tag{2.16}$$

where

$$\lambda \equiv U'_{\mathrm{B}}(0) \tag{2.17}$$

is equal to 0.3321... for the Blasius boundary layer.

2.2. *The unsteady flow*

We suppose that the time t has been normalized by l/U_∞ and put

$$x = x^*/l. \tag{2.18}$$

Then the unsteady flow is governed by the linearized Navier–Stokes equations

$$u_t + U_0 u_x + u U_{0x} + \epsilon^{-4}(v U_{0y} + V_0 u_y) = -p_x + u_{yy} + \epsilon^8 u_{xx}, \tag{2.19}$$

$$v_t + U_0 v_x + u V_{0x} + \epsilon^{-4}(v V_{0y} + V_0 v_y) = -\epsilon^{-4} p_y + v_{yy} + \epsilon^8 v_{xx}, \tag{2.20}$$

$$u_x + \epsilon^{-4} v_y = 0. \tag{2.21}$$

Since the problem is linear, the entire unsteady flow will have harmonic time dependence, and we can put

$$\left.\begin{aligned} u &= \mathrm{e}^{-\mathrm{i}St}\,\tilde{u}(x,y), \\ v &= \mathrm{e}^{-\mathrm{i}St}\,\tilde{v}(x,y), \\ p &= \mathrm{e}^{-\mathrm{i}St}\,\tilde{p}(x,y), \end{aligned}\right\} \tag{2.22}$$

where

$$S = \omega l/U_\infty$$

is the Strouhal number and, since the body is assumed to be thin,

$$\tilde{u} \to 1 \quad \text{as } y \to \infty, \tag{2.23}$$

to the lowest approximation.

Upstream of the triple deck, where the mean flow changes on the scale of x, the unsteady flow in the boundary layer is given by the Stokes solution

$$\left.\begin{aligned} \tilde{u} &= 1 - \exp\left[\mathrm{i}^{\frac{3}{2}} S^{\frac{1}{2}} y\right], \\ \tilde{p} &= \mathrm{i}Sx. \end{aligned}\right\} \tag{2.24}$$

Our interest here is in the relatively high-frequency case, where ω is of the order of the Tollmien–Schlichting wave frequency at and upstream of the lower branch of the neutral-stability curve. The analyses of Goldstein (1983*a*,*b*) and Smith (1973) show that S must then be $O(\epsilon^{-2})$, so that

$$S_0 \equiv \epsilon^2 S \tag{2.25}$$

will be $O(1)$. The Stokes-layer thickness will then be the same as that of the lower deck, and (2.24) can be written as

$$\tilde{p} = \mathrm{i}\epsilon S_0 X, \tag{2.26}$$

$$\tilde{u} = \begin{cases} 1 & \text{for } y = O(1) \\ 1 - \mathrm{e}^{\mathrm{i}^{\frac{3}{2}} S_0^{\frac{1}{2}} Y} & \text{for } Y = O(1). \end{cases} \tag{2.27}$$

The abrupt streamwise variations in the mean flow will modify this solution within the triple deck, and in the main deck the unsteady solution will be of the form

$$\left.\begin{aligned}\tilde{u} &= \tilde{u}_0(X,y)+\epsilon\tilde{u}_1(X,y)+\ldots,\\ \tilde{v} &= \epsilon\tilde{v}_0(X,y)+\epsilon^2\tilde{v}_1(X,y)+\ldots,\\ \tilde{p} &= \epsilon\tilde{p}_0(X,y)+\epsilon^2\tilde{p}_1(X,y)+\ldots.\end{aligned}\right\} \tag{2.28}$$

Substituting these via (2.22) into the linearized Navier–Stokes equations, using (2.6) and (2.7) and equating to zero the coefficients of ϵ^{-3} yields

$$U_{\mathrm{B}}\tilde{u}_{0X}+\tilde{v}_0\,U'_{\mathrm{B}}=0, \tag{2.29}$$

$$\tilde{u}_{0X}=-\tilde{v}_{0y}, \tag{2.30}$$

$$\tilde{p}_{0y}=0. \tag{2.31}$$

Hence, using (2.23) and (2.27) and the fact that $U'_{\mathrm{B}}\to 0$ as $y\to\infty$, we find that

$$\tilde{u}_0 = 1+a(X)U'_{\mathrm{B}}(y), \tag{2.32}$$

$$\tilde{v}_0 = -a'(X)U_{\mathrm{B}}(y), \tag{2.33}$$

$$\tilde{p}_0 = p_0(X), \tag{2.34}$$

where

$$a(X)\to 0 \quad \text{as } X\to-\infty, \tag{2.35}$$

and it follows from (2.26) that†

$$p_0(X)\to \mathrm{i}S_0X \quad \text{as } X\to-\infty. \tag{2.36}$$

In the upper deck, where

$$\hat{y}\equiv\epsilon y \tag{2.37}$$

is $O(1)$, (2.23) implies that the solution will be of the form

$$\left.\begin{aligned}\tilde{u} &= 1+\epsilon\hat{u}_1(X,\hat{y})+\ldots,\\ \tilde{v} &= \epsilon\hat{v}_1(X,\hat{y})+\ldots,\\ \tilde{p} &= \epsilon\hat{p}_1(X,\hat{y})+\ldots.\end{aligned}\right\} \tag{2.38}$$

Substituting this into (2.19) and (2.20) via (2.22) and using (2.25) and the fact that $(U_0, V_0)=(1,0)+O(\epsilon)$ in the upper deck, we find that $\hat{p}_1-\mathrm{i}S_0X$ and $\hat{v}_1$ are conjugate harmonic functions (i.e. the real and imaginary parts of an analytic function of the complex variable $X+\sqrt{-1}\,\hat{y}$). Matching with the main-deck solutions (2.32) to (2.34) shows that

$$\hat{v}_1(X,0)=-a'(X) \quad \text{and} \quad \hat{p}_1(X,0)=p_0(X).$$

It follows that

$$a''(X)=\frac{1}{\pi}\int_{-\infty}^{\infty}\frac{p'_0(\bar{X})-\mathrm{i}S_0}{\bar{X}-X}\,\mathrm{d}\bar{X}. \tag{2.39}$$

Finally, the solution in the lower deck is of the form

$$\left.\begin{aligned}\tilde{u} &= u_0(X,Y)+O(\epsilon),\\ \tilde{v} &= \epsilon^2 v_0(X,Y)+O(\epsilon^3),\\ \tilde{p} &= \epsilon p_0(X)+O(\epsilon^2).\end{aligned}\right\} \tag{2.40}$$

† Complete matching with the upstream solution may require that we introduce an unsteady foredeck such as that used by Brown & Daniels (1975) for the unsteady trailing-edge problem. But it turns out that we can obtain the solutions to the required degree of accuracy without actually doing this.

Substituting these into (2.19) and (2.20) via (2.22), using (2.11) and (2.25) and equating to zero coefficients of ϵ^{-2}, we find that u_0 and v_0 satisfy the linearized unsteady boundary-layer equations

$$-\mathrm{i}S_0 u_0 + Uu_{0X} + u_0 U_X + v_0 U_Y + Vu_{0Y} = -p_0' + u_{0YY}, \tag{2.41}$$

$$u_{0X} = -v_{0Y}. \tag{2.42}$$

At the wall u_0 and v_0 satisfy the no-slip boundary condition

$$u_0 = v_0 = 0 \quad \text{for } Y = hF(X), \tag{2.43}$$

and matching with (2.27) and (2.32) shows that

$$u_0 \to 1 - \mathrm{e}^{\mathrm{i}\frac{3}{2}S_0^{\frac{1}{2}}Y} \quad \text{as } X \to -\infty \tag{2.44}$$

and

$$u_0 \to 1 + \lambda a(X) \quad \text{as } Y \to \infty, \tag{2.45}$$

where λ is defined by (2.17).

This completes the formulation of the problem. The entire unsteady solution will be known once the solution of (2.41) and (2.42) subject to the conditions (2.39) and (2.43) to (2.45) has been obtained. But this requires that the solution of the corresponding steady problem (2.12)–(2.16) be found, which has only been done numerically (Ragab & Nayfeh 1980; Sykes 1978; Napolitans, Werle & Davis 1979).

Fortunately, much of the physics of the receptivity phenomenon is best understood by considering the linearized solution corresponding to moderately large curvature, i.e. to $h \ll 1$ in (2.3). This is done in §3.

3. The linearized solution

We begin by considering the steady problem (2.12)–(2.16). Its solution has already been obtained by Stewartson (1970, 1971). For convenience we summarize his results in the present notation.

3.1. *The steady solution*

The linearized solution for $h \ll 1$ is given by (Stewartson 1970, 1971)

$$U = \lambda Y + hU^{(1)}, \tag{3.1}$$

$$V = hV^{(1)}, \tag{3.2}$$

$$A = hA^{(1)}, \tag{3.3}$$

$$P' = hQ^{(1)}, \tag{3.4}$$

where the Fourier transforms with respect to X, say $\bar{U}$, $\bar{V}$, $\bar{A}$ and $\bar{Q}$, of the perturbation quantities $U^{(1)}$, $V^{(1)}$, $A^{(1)}$ and $Q^{(1)}$ respectively, e.g.

$$\bar{U}(Y) = \frac{1}{(2\pi)^{\frac{1}{2}}} \int_{-\infty}^{\infty} U^{(1)}(X, Y)\, \mathrm{e}^{-\mathrm{i}kX}\, \mathrm{d}X \tag{3.5}$$

satisfy

$$\bar{U}''' = \mathrm{i}k\lambda Y \bar{U}', \tag{3.6}$$

$$\bar{U}(0) = -\lambda \bar{F}, \tag{3.7}$$

$$\left.\begin{aligned} &\bar{U} \to \lambda \bar{A} \quad \text{as } Y \to \infty, \\ &\bar{A} = -\mathrm{i}\frac{[(k+\mathrm{i}0)(k-\mathrm{i}0)]^{\frac{1}{2}}}{k^3}\bar{Q}, \end{aligned}\right\} \tag{3.8}$$

$$\bar{V} = \frac{1}{\lambda}(\bar{U}'' - \bar{Q}) - ik\bar{U}Y, \tag{3.9}$$

$$\bar{V}(0) = 0, \tag{3.10}$$

where $\bar{F}$ denotes the Fourier transform of F (in the notation (3.5)), $k \pm \mathrm{i}0$ indicates that a small positive/negative imaginary quantity (which is ultimately put equal to zero) has been added to k, and the branch cuts of $(k \pm \mathrm{i}0)^{\frac{1}{3}}$ are to be taken in the lower/upper half-planes.

The solution to (3.6)–(3.10) is given by

$$\bar{U}' = \frac{\lambda \bar{F}(k)\,(\mathrm{i}k\lambda)^{\frac{1}{3}}}{D(k)} \operatorname{Ai}[(\mathrm{i}k\lambda)^{\frac{1}{3}} Y], \tag{3.11}$$

$$\bar{Q} = -\frac{\lambda \bar{F}(k)\,(\mathrm{i}k\lambda)^{\frac{2}{3}}}{D(k)\,3^{\frac{1}{3}}\Gamma(\frac{1}{3})}, \tag{3.12}$$

where $\arg(\mathrm{i}k\lambda)^{\frac{1}{3}} = \pm\frac{1}{6}\pi$ for $k \gtrless 0$, we have put

$$D(k) \equiv \frac{1}{3} - \frac{\mathrm{i}\lambda(\mathrm{i}k\lambda)^{\frac{2}{3}}}{\gamma(k)\,3^{\frac{1}{3}}\Gamma(\frac{1}{3})}, \tag{3.13}$$

$$\gamma \equiv \frac{k^3}{[(k+\mathrm{i}0)\,(k-\mathrm{i}0)]^{\frac{1}{2}}}, \tag{3.14}$$

and Γ denotes the gamma function.

3.2. *The unsteady solution*

As already indicated, the analysis in this section is similar to the linearized study of Brown & Daniels (1975). Corresponding to the expansion (3.1)–(3.4) of the steady solution, the unsteady solution of (2.41)–(2.45) and (2.39) can be expressed as

$$u_0 = 1 - \mathrm{e}^{\mathrm{i}^{\frac{3}{2}} S_0^{\frac{1}{2}} Y} + h u^{(1)}, \tag{3.15}$$

$$v_0 = h v^{(1)}, \tag{3.16}$$

$$a = h a^{(1)}, \tag{3.17}$$

$$p_0' = \mathrm{i}S_0 + h q^{(1)}(X), \tag{3.18}$$

where terms $O(h^2)$ are again neglected. Substituting these together with (3.1) and (3.2) into (2.41)–(2.45) and equating to zero like powers of h yields, upon transferring (2.43) to $Y = 0$,

$$-\mathrm{i}S_0 u^{(1)} + \lambda(Y u_X^{(1)} + v^{(1)}) + q^{(1)} - u_{YY}^{(1)} = -(1 - \mathrm{e}^{\mathrm{i}^{\frac{3}{2}} S_0^{\frac{1}{2}} Y})\, U_x^{(1)} + \mathrm{i}^{\frac{3}{2}} S_0^{\frac{1}{2}} \mathrm{e}^{\mathrm{i}^{\frac{3}{2}} S_0^{\frac{1}{2}} Y} V^{(1)}, \tag{3.19}$$

$$u_X^{(1)} + v_Y^{(1)} = 0, \tag{3.20}$$

$$u^{(1)} = \mathrm{i}^{\frac{3}{2}} S_0^{\frac{1}{2}} F(X), \quad v^{(1)} = 0 \quad \text{for } Y = 0, \tag{3.21}$$

$$u^{(1)} \to 0 \quad \text{as } X \to -\infty, \tag{3.22}$$

$$u^{(1)} \to \lambda a^{(1)} \quad \text{as } Y \to \infty. \tag{3.23}$$

Equation (2.39) shows that

$$\frac{\mathrm{d}^2 a^{(1)}}{\mathrm{d}X^2} = \frac{1}{\pi} \int_{-\infty}^{\infty} \frac{q^{(1)}(\tilde{X})}{\tilde{X} - X}\, \mathrm{d}\tilde{X}. \tag{3.24}$$

Differentiating (3.19) with respect to Y, using (3.20), and noting that $U^{(1)}$ and $V^{(1)}$ also satisfy this equation, we obtain

$$\mathrm{i}S_0 u_Y^{(1)} - \lambda Y u_{XY}^{(1)} + u_{YYY}^{(1)} = (1 - \mathrm{e}^{\mathrm{i}^{\frac{3}{2}} S_0^{\frac{1}{2}} Y})\, U_{XY}^{(1)} + \mathrm{i}S_0 \mathrm{e}^{\mathrm{i}^{\frac{3}{2}} S_0^{\frac{1}{2}} Y} V^{(1)}. \tag{3.25}$$

It follows from (3.21)–(3.25) that the Fourier transforms with respect to X, say $\bar{u}$, $\bar{v}$, $\bar{a}$ and $\bar{q}$, of the perturbation variables $u^{(1)}$, $v^{(1)}$, $a^{(1)}$ and $q^{(1)}$ respectively, e.g.

$$\bar{u}(Y) = \frac{1}{(2\pi)^{\frac{1}{2}}} \int_{-\infty}^{\infty} u^{(1)}(X, Y)\, \mathrm{e}^{-\mathrm{i}kX}\, \mathrm{d}X, \tag{3.26}$$

satisfy

$$\bar{u}''' + \mathrm{i}(S_0 - k\lambda Y)\, \bar{u}' = \mathrm{i}k(1 - \mathrm{e}^{\mathrm{i}^{\frac{3}{2}} S_0^{\frac{1}{2}} Y})\, \bar{U}' + \mathrm{i}S_0 \mathrm{e}^{\mathrm{i}^{\frac{3}{2}} S_0^{\frac{1}{2}} Y}\, \bar{V}, \tag{3.27}$$

$$\bar{u}(0) = \mathrm{i}^{\frac{3}{2}} S_0^{\frac{1}{2}}\, \bar{F}, \tag{3.28}$$

$$\bar{v}(0) = 0, \tag{3.29}$$

$$\bar{u} \to \lambda \bar{a} \quad \text{as } Y \to \infty, \tag{3.30}$$

$$\bar{q} = \mathrm{i}\gamma \bar{a}, \tag{3.31}$$

where γ is defined by (3.14). Hence it follows from (3.10) and (3.19) that

$$\bar{u}''(0) = \mathrm{i}\gamma \bar{a} + \mathrm{i}^{\frac{1}{2}} S_0^{\frac{3}{2}}\, \bar{F}. \tag{3.32}$$

Putting

$$\bar{u} = \bar{u}_1 + \frac{k\bar{U}}{S_0} + \frac{\mathrm{i}S_0}{\lambda} \int_0^Y \mathrm{e}^{\mathrm{i}^{\frac{3}{2}} S_0^{\frac{1}{2}} Y}\, \bar{U}\, \mathrm{d}Y \tag{3.33}$$

and using (3.9) to eliminate $\bar{V}$ on the right-hand side of (3.27), we find that $\bar{u}_1$ satisfies

$$\bar{u}_1''' + \mathrm{i}(S_0 - k\lambda Y)\, \bar{u}_1' = -\mathrm{i}kG(Y), \tag{3.34}$$

where we have put

$$G(Y) \equiv \mathrm{e}^{\mathrm{i}^{\frac{3}{2}} S_0^{\frac{1}{2}} Y} \left[(2\zeta_0^3 + 1)\, \bar{U}' + \frac{S_0}{k\lambda} \bar{Q} \right] \tag{3.35}$$

and

$$\zeta_0 \equiv \frac{S_0}{(\mathrm{i}k\lambda)^{\frac{2}{3}} \mathrm{i}} = \frac{S_0}{(k\lambda)^{\frac{2}{3}}} \mathrm{e}^{-\frac{1}{6}\mathrm{i}\pi}. \tag{3.36}$$

Since (3.34) possesses homogeneous solutions whose first derivatives are $\mathrm{Ai}(\zeta)$ and $\mathrm{Bi}(\zeta)$, where

$$\zeta \equiv (\mathrm{i}k\lambda)^{\frac{1}{3}} Y + \zeta_0, \tag{3.37}$$

it follows that the solution to (3.34) that remains bounded as $Y \to \infty$ is given by

$$\bar{u}_1' = -\frac{(\mathrm{i}k\lambda)^{\frac{2}{3}} \pi}{\lambda} \left[\mathrm{Bi}(\zeta) \int_{\infty}^{Y} \mathrm{Ai}(\tilde{\zeta})\, G(\tilde{Y})\, \mathrm{d}\tilde{Y} - \mathrm{Ai}(\zeta) \int_0^Y \mathrm{Bi}(\tilde{\zeta})\, G(\tilde{Y})\, \mathrm{d}\tilde{Y} \right] + C(k)\, \mathrm{Ai}(\zeta). \tag{3.38}$$

Substituting this into (3.33), inserting the result into the boundary conditions (3.28), (3.30) and (3.32), integrating by parts to simplify the double integral, using (3.7)–(3.10) to eliminate $\bar{U}(0)$, $\bar{U}(\infty)$ and $\bar{U}''(0)$, and solving for $\bar{a}$, we find that

$$\bar{a} = \frac{k}{S_0} \bar{A} + \frac{S_0}{\lambda\gamma} \bar{U}'(0) + \frac{S_0\, \mathrm{Ai}'(\zeta_0)}{\lambda\gamma\zeta_0 \Delta} \left\{ (\mathrm{i}k\lambda)^{\frac{1}{3}} \int_0^{\infty} [K(\zeta, \zeta_0)\, G(Y) - \mathrm{e}^{\mathrm{i}^{\frac{3}{2}} S_0^{\frac{1}{2}} Y} \zeta_0^{\frac{1}{2}}\, \bar{U}'(Y)]\, \mathrm{d}Y + \frac{k\lambda^2 \bar{F}}{S_0} - \frac{S_0 \lambda}{\gamma} \bar{U}'(0) \right\}, \tag{3.39}$$

where

$$K(\zeta, \zeta_0) \equiv \pi \frac{\mathrm{Ai}'(\zeta_0)\, \mathrm{Gi}(\zeta) - \mathrm{Gi}'(\zeta_0)\, \mathrm{Ai}(\zeta)}{\mathrm{Ai}'(\zeta_0)}, \tag{3.40}$$

$$\Delta \equiv \int_{\zeta_0}^{\infty} \mathrm{Ai}(\zeta)\, \mathrm{d}\zeta + \frac{S_0 \lambda}{\gamma} \frac{\mathrm{Ai}'(\zeta_0)}{\zeta_0}, \tag{3.41}$$

and Gi and Gi′ denote the combinations of Airy functions and Airy-function integrals defined on p. 448 of Abramowitz & Stegun (1964).

It follows from (3.32) and (3.33) that $C(k)$ is now given by

$$C(k) = \frac{\mathrm{i}}{(\mathrm{i}k\lambda)^{\frac{1}{3}}\,\mathrm{Ai}'(\zeta_0)}\left[\gamma\left(\bar{a}-\frac{k}{S_0}\bar{A}\right)-\frac{S_0}{\lambda}\bar{U}'(0)-k\pi\,\mathrm{Bi}'(\zeta_0)\int_0^\infty \mathrm{Ai}(\zeta)\,G(Y)\,\mathrm{d}Y\right]. \quad (3.42)$$

Substituting (3.11), (3.12) and (3.35) into (3.39), changing the variable of integration, and deforming the contour yields

$$\bar{a} = \frac{k}{S_0}\bar{A}+\frac{S_0}{\lambda\gamma}\bar{U}'(0)-\frac{\bar{F}k\lambda\,\mathrm{Ai}'(\zeta_0)}{\gamma\Delta D}\left\{\int_0^\infty \mathrm{e}^{-\zeta_0^{\frac{1}{2}}\tau}\left[K(\tau+\zeta_0,\zeta_0)\,g(\tau,\zeta_0)\right.\right.$$
$$\left.\left.-\zeta_0^{\frac{1}{2}}\,\mathrm{Ai}(\tau)\right]\mathrm{d}\tau-\frac{D}{\zeta}-\frac{S_0\lambda}{\gamma 3^{\frac{2}{3}}\Gamma(\frac{2}{3})}\right\}, \quad (3.43)$$

where we have put

$$g(\tau,\zeta_0) \equiv (2\zeta_0^{\frac{3}{2}}+1)\,\mathrm{Ai}(\tau)+\frac{\zeta_0}{3^{\frac{1}{3}}\Gamma(\frac{1}{3})}, \quad (3.44)$$

and the integral can be carried out along the real axis. This essentially completes the solution to the problem. Physical quantities can be found by inserting (3.42) and (3.43) into (3.33) and (3.38), and inverting the Fourier transforms of the type (3.26). We are, however, only interested in the amplitude of the Tollmien–Schlichting wave produced by the interaction, and not in the complete solution. Fortunately the former is much easier to calculate than the latter.

4. Coupling coefficient – the receptivity problem

Bogdanova & Ryzhov (1983) analysed the generation of instabilities by pistons in plane Poiseuille flow, and Goldstein (1984) analysed the generation of instabilities by external disturbances in flows separating from smooth surfaces. Both of these are related to the present work (and to Goldstein 1983*a*) in that they involve viscid–inviscid interactions. The first of these, being concerned with input disturbances that are already of the appropriate Tollmien–Schlichting wavelength scale, is more closely related to the Nishioka & Morkovin (1985) study (referred to in §1) than to the present analysis or to Shapiro's (1977) experiment.

It follows from (3.17) and (3.26) that

$$a(X) = \frac{h}{(2\pi)^{\frac{1}{2}}}\int_{-\infty}^{\infty}\mathrm{e}^{\mathrm{i}kX}\,\bar{a}(k)\,\mathrm{d}k. \quad (4.1)$$

Our interest is in the region downstream of the interaction zone (i.e. the region of large surface curvature) where $X > 0$. Then the integration contour can be closed in the upper half-plane.

Equation (3.43) shows that the integrand possesses poles at points where

$$\Delta = 0. \quad (4.2)$$

But it follows from (3.14), (3.36) and (3.41) that (4.2) is just the lowest-order approximation to the characteristic equation obtained from the classical large-Reynolds-number–small-wavenumber asymptotic solution to the Orr–Sommerfeld equation for the region near the lower branch of the neutral-stability curve (Lin 1946, p. 294 of Appendix and the equation immediately following (12.5)†; Reid 1965, pp. 279–282). Its roots are the eigenvalues of the Orr–Sommerfeld equation corresponding to the Tollmien–Schlichting waves. This is to be expected since, as was

† There are some minor typographical errors in equation (7) of Lin's Appendix, and a prime is missing in his equation (12.5).

shown by Smith (1979) and Goldstein (1983), the Tollmien–Schlichting waves exhibit the same triple-deck structure as the present solution in the region upstream of the lower branch of the neutral-stability curve.

We suppose that the interaction zone lies upstream of this curve, so that the Tollmien–Schlichting waves initially decay. (Goldstein (1983*a*,*b*) showed that (4.2) is the correct characteristic equation for these waves everywhere in this upstream region.) Then the roots of (4.2) must lie in the first quadrant of the k-plane, and we can put

$$\gamma = k^2. \tag{4.3}$$

We are only interested in the root corresponding to the Tollmien–Schlichting wave that ultimately exhibits spatial growth in the downstream region (i.e. its lowest-order root, see Goldstein 1983*a*,*b*). The contribution a_{TS} to (4.1) from the corresponding pole is just equal to $2\pi\mathrm{i}$ times the residue of the integrand at this point, which we denote by $k = \kappa$ (Goldstein 1981). Then, denoting the corresponding value of ζ_0 by η so that

$$\kappa = \frac{S_0^3}{\lambda\eta^{\frac{3}{2}}\,\mathrm{e}^{\frac{1}{4}\mathrm{i}\pi}} \tag{4.4}$$

and

$$\Lambda(\eta) = \int_\eta^\infty \mathrm{Ai}\,(\zeta)\,\mathrm{d}\zeta + \mathrm{i}\left(\frac{\eta\lambda^{\frac{3}{2}}}{S_0}\right)^2 \mathrm{Ai}'\,(\eta) \equiv 0, \tag{4.5}$$

we find from (3.43) that

$$a_{\mathrm{TS}}(X) = \lambda h\,\mathrm{e}^{\mathrm{i}\kappa X}\,\bar{F}(\kappa)\,\Lambda(S_0/\lambda^{\frac{3}{2}}), \tag{4.6}$$

where we have put

$$\Lambda = \frac{3\mathrm{i}\,(2\pi)^{\frac{1}{2}}\,\mathrm{Ai}'\,(\eta)}{2\,\eta D(\eta)\,\Lambda'(\eta)}\left\{\int_0^\infty \mathrm{e}^{-\eta^{\frac{1}{2}}\tau}\,[K(\tau+\eta,\eta)\,g(\tau,\eta) - \eta^{\frac{1}{2}}\,\mathrm{Ai}\,(\tau)]\,\mathrm{d}\tau - \frac{D}{\eta} - \frac{\mathrm{i}(\lambda\eta)^3}{3^{\frac{2}{3}}S_0^2\,\Gamma(\frac{2}{3})}\right\}; \tag{4.7}$$

Λ' denotes the derivative of (4.5) with respect to η, and it follows from (3.13), (4.3) and (4.4) that

$$D(\eta) = \tfrac{1}{3} - \mathrm{i}\left(\frac{\eta\lambda^{\frac{3}{2}}}{S_0}\right)^2 \frac{1}{3^{\frac{1}{3}}\Gamma(\frac{1}{3})}. \tag{4.8}$$

Equations (2.22) and (2.32) therefore imply that the streamwise velocity fluctuation produced by the Tollmien–Schlichting wave is given by

$$u_{\mathrm{TS}} = \lambda h\bar{F}(\kappa)\,\Lambda\left(\frac{S_0}{\lambda^{\frac{3}{2}}}\right)\mathrm{e}^{\mathrm{i}(\kappa X - St)}\,U_{\mathrm{B}}'(y) \quad \text{for } y = O(1) \tag{4.9}$$

in the main part of the boundary layer. Similarly (2.38), (2.40), (3.15), (3.26), (3.33), (3.38) and (3.42) imply that the streamwise velocity fluctuation in the lower deck is given by

$$u_{\mathrm{TS}} = \lambda h\bar{F}(\kappa)\,\Lambda\left(\frac{S_0}{\lambda^{\frac{3}{2}}}\right)\mathrm{e}^{\mathrm{i}(\kappa X - St)}\,\lambda\frac{\displaystyle\int_\eta^{(\mathrm{i}\kappa\lambda)^{\frac{1}{3}}Y+\eta} \mathrm{Ai}\,(\zeta)\,\mathrm{d}\zeta}{\displaystyle\int_\eta^\infty \mathrm{Ai}\,(\zeta)\,\mathrm{d}\zeta} \quad \text{for } Y = O(1). \tag{4.10}$$

At larger values of the scaled frequency parameter $S_0/\lambda^{\frac{3}{2}}$ the root κ of $\Lambda = 0$ crosses into the lower half-plane, and the Tollmien–Schlichting wave then begins to grow, but, as explained by Goldstein (1981) on the basis of causality arguments and more recently by Bogdanova & Ryzhov (1983) from a somewhat different point of view, the Fourier-inversion contour in (4.1) must then be deformed to lie below the corresponding pole in the integrand. The net result is that the preceding formulas (e.g. (4.9) and (4.10)) apply without modification.

By using equations (10.4.9), (10.4.42) and (10.4.43) on pp. 446 and 448 of Abramowitz & Stegun (1964) to eliminate Gi and Bi, (3.40) can be written as

$$K(\tau+\eta,\eta)=\frac{2\pi}{\mathrm{i}}\left\{\mathrm{Ai}\,(\tau+\eta)\left[\int_{\infty}^{(\tau+\eta)\,\mathrm{e}^{\frac{2}{3}\mathrm{i}\pi}}\mathrm{Ai}\,(s)\,\mathrm{d}s+\Delta(\eta\,\mathrm{e}^{\frac{2}{3}\mathrm{i}\pi})\right]\right.$$
$$\left.-\mathrm{e}^{\frac{2}{3}\mathrm{i}\pi}\,\mathrm{Ai}\,((\tau+\eta)\,\mathrm{e}^{\frac{2}{3}\mathrm{i}\pi})\int_{\infty}^{\tau+\eta}\mathrm{Ai}\,(s)\,\mathrm{d}s\right\}. \quad (4.11)$$

It therefore follows from the asymptotic expansions of the Airy functions that

$$K(\tau+\eta,\eta)\to\frac{1}{\tau+\eta}+\frac{\pi^{\frac{1}{2}}}{\mathrm{i}}\Delta(\eta\,\mathrm{e}^{\frac{2}{3}\mathrm{i}\pi})\frac{\mathrm{e}^{-\frac{2}{3}(\tau+\eta)^{\frac{3}{2}}}}{(\tau+\eta)^{\frac{1}{4}}}\quad\text{as }\tau+\eta\to\infty \quad (4.12)$$

and that the lowest-order root η of (4.2) (with Δ defined in (3.41)) behaves like

$$\eta\to\frac{S_0^{\frac{2}{3}}}{\lambda}\left(\mathrm{e}^{-\frac{1}{6}\mathrm{i}\pi}-\frac{\lambda^{\frac{1}{2}}\,\mathrm{e}^{\frac{5}{12}\mathrm{i}\pi}}{3S_0}\right)+\ldots\quad\text{as }S_0\to\infty. \quad (4.13)$$

Hence $$\Delta'(\eta)\to\frac{3}{\eta^2}\,\mathrm{Ai}'\,(\eta),\quad \Delta(\eta\,\mathrm{e}^{\frac{2}{3}\mathrm{i}\pi})\propto\frac{\mathrm{e}^{\frac{2}{3}\eta^{\frac{3}{2}}}}{\eta^{\frac{9}{4}}}\quad\text{as }S_0\to\infty.$$

Inserting these results into (4.7) and using (3.44) and (4.8), we find that

$$\Lambda\left(\frac{S_0^{\frac{2}{3}}}{\lambda}\right)\to-(\tfrac{1}{2}\pi)^{\frac{1}{2}}\mathrm{i}\quad\text{as }S_0\to\infty. \quad (4.14)$$

Substituting this along with (4.4) and (4.13) into (4.9) yields

$$u_{\mathrm{TS}}\to-\lambda\mathrm{i}\,(\tfrac{1}{2}\pi)^{\frac{1}{2}}h\bar{F}((\lambda S_0)^{\frac{1}{2}})\,\mathrm{e}^{\mathrm{i}((\lambda S_0)^{\frac{1}{2}}X-St)}\,U_{\mathrm{B}}'(y)\quad\text{as }S_0\to\infty. \quad (4.15)$$

5. Discussion of results

In the absence of the large-curvature region, the imposed disturbance would produce only a Stokes shear flow, which is independent of both the mean boundary layer and the streamwise coordinate to lowest order. The Stokes layer (across which this flow adjusts to the free stream) is very thin – of the order of the lower-deck thickness ϵ^5 – when the disturbance frequency is of the order of the Tollmien–Schlichting wave frequency for the lower branch of the neutral-stability curve, i.e. when the Strouhal number is $O(\epsilon^{-2})$. The Stokes solution results from the balance of the $O(\epsilon^{-2})$ pressure, viscous and temporal acceleration terms in the linearized momentum equation – the convective acceleration terms being negligible to this order. But the large curvature in the interaction region induces a cross-stream mean-velocity component V_0, which is $O(\epsilon^3)$ in the lower deck. This in turn introduces a convective acceleration term $\epsilon^{-4}\,V_0\,\partial u/\partial y=O(\epsilon^{-2})$ in the lower-deck linearized streamwise momentum equation, which is of the same order as the pressure, temporal acceleration and viscous terms. Then since V_0 depends on $X=x/\epsilon^3$, this causes the initial Stokes-type solution to exhibit an X-dependence that is of the same scale, namely $O(\epsilon^3 l)$, as the Tollmien–Schlichting wavelength at the lower branch of the neutral-stability curve. In this way the very small ($O(\epsilon^2)$) mean-flow variation across the interaction region is able to 'scatter' the imposed disturbance into a Tollmien–Schlichting wave that has roughly the same amplitude as that disturbance.

Most of Shapiro's (1977) experiments were carried out at a frequency parameter $\omega\nu/U_\infty^2$ of 0.56×10^{-4}, so that his *theoretical* flat-plate neutral-stability point corres-

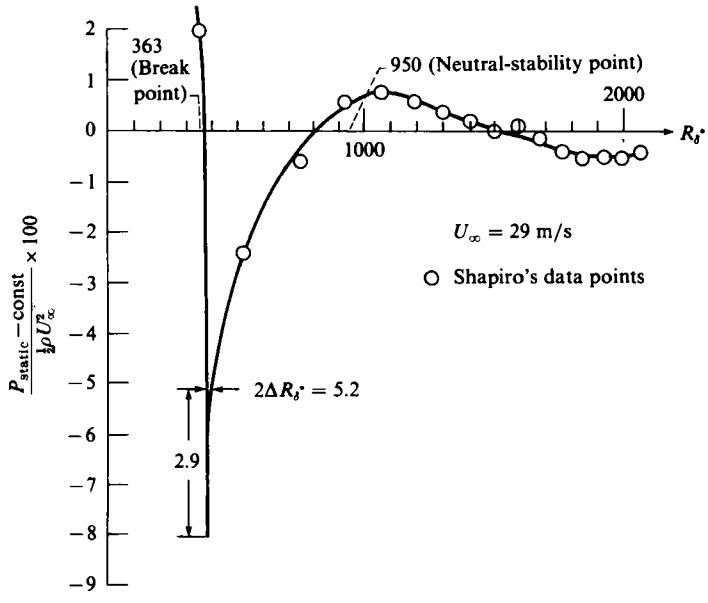

FIGURE 4. Static-pressure distribution as a function of R_δ^* measured by Shapiro.

ponded to a displacement-thickness Reynolds number R_δ^* (in Shapiro's notation) of roughly 9.5×10^2 (according to Shapiro). Our parameters ϵ and S_0, which are equal to $(R_\delta^*/1.72)^{-\frac{1}{4}}$ and $(R_\delta^*/1.72)^{\frac{3}{4}}\,\omega\nu/U_\infty^2$ respectively, are therefore about 0.2 and 0.73 respectively at his neutral-stability point. The 'nose' region of his plate appears to end at about 0.21 cm from the leading edge. This corresponds to an R_δ^* of 363 for the experiments run at 29 m/s, so that $\epsilon \approx 0.26$ and $S_0 \approx 0.17$ in this case.

Figure 4 is a reproduction of Shapiro's (1977) measured static-pressure distribution plotted as a function of R_δ^* (his figure 25). The only difference is that we have put a slightly different curve through his data points in the vicinity of the break point (i.e. the end of the nose region). Since $\Delta R_\delta^* \approx 0.86\,\Delta X/\epsilon$ there, $2\,\Delta X$ will equal 1.56 when $2\,\Delta R_\delta^* = 5.2$. The magnitude of the negative peak lying below this width is roughly $\Delta P_0 \approx 1.45 \times 10^{-2}$. (Notice that Shapiro's normalized pressure levels are twice ours, owing to differences in normalization.) This corresponds to a $\Delta P = \Delta P_0/\epsilon^2$ of about 0.21. Inspection of Stewartson's (1971) figure 2(*a*) reveals that his theoretical negative static-pressure distribution peaks at almost exactly that value and that the peak has a width $2\,\Delta X$ of about 1.5 where his curve crosses the real axis. This shows that Shapiro's static-pressure measurements are compatible with the predictions of the present theory when $\alpha_0 \equiv \alpha/h\epsilon^2$, the scaled turning across the interaction region, is equal to unity.

The most important results of the present study are equations (4.9) and (4.10) for the Tollmien–Schlichting velocity fluctuations generated downstream of the interaction region. The factor $\lambda h\bar{F}\Lambda$ is a measure of the amplitude of the Tollmien-Schlichting wave to that of the imposed disturbance. Following Tam (1971), we refer to it as the 'coupling coefficient'.

The factor $\Lambda(S\epsilon^2/\lambda^{\frac{3}{2}})$ is independent of the geometry of the interaction region and depends on the upstream boundary layer only through the scaled skin friction just upstream of the interaction region. Λ is plotted against $S\epsilon^2/\lambda^{\frac{3}{2}}$ in figure 5. Its asymptotic limit (4.14) is indicated by the dashed line. The figure shows that the

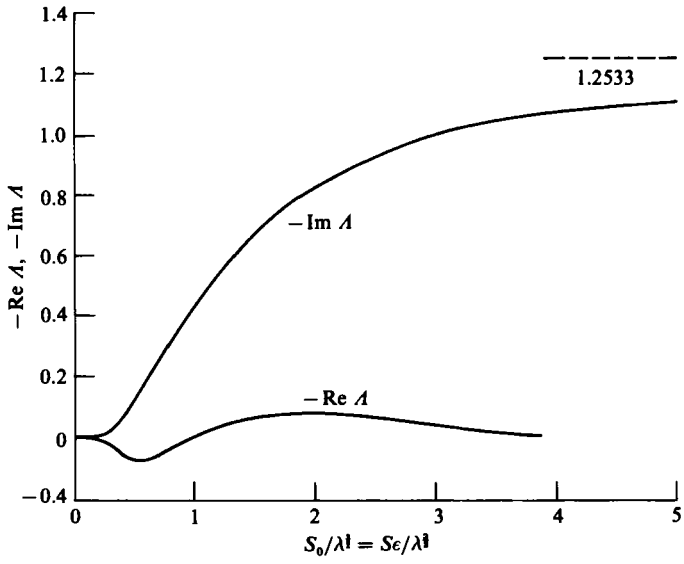

FIGURE 5. Real and imaginary parts of Λ.

in-phase component (real part) is generally small compared with the out-of-phase component, which monotonically increases to its limiting value of about unity. Thus Λ merely produces a net phase shift of $-\frac{1}{2}\pi$ between the free-stream disturbance and the Tollmien–Schlichting wave, at sufficiently large values of the scaled frequency parameter $S_0/\lambda^{\frac{1}{3}}$.

The interaction-region geometry is accounted for through the factor $h\bar{F}$, which, for a given geometry, depends only on the complex Tollmien–Schlichting wavenumber κ. In order to get some idea about the magnitude of $\bar{F}(\kappa)$, we evaluate it for the discontinuous slope change in which

$$F = 0, -\alpha_0 X \quad \text{for } X < 0,\ X > 0.$$

Inserting this into (3.26) yields

$$h\bar{F}(k) = \frac{h\alpha_0}{(2\pi)^{\frac{1}{2}}(k-i_0)^2}, \tag{5.1}$$

so that (4.4) implies that

$$h\bar{F}(\kappa) = \frac{\mathrm{i}h\alpha_0}{(2\pi)^{\frac{1}{2}}}\left(\frac{\lambda^{\frac{1}{3}}\eta}{S_0}\right)^3. \tag{5.2}$$

5.1. *Some rough order-of-magnitude estimates and comparison with the infinitely thin flat plate*

Equations (4.9) and (4.10) have to be corrected for mean-flow divergence effects when the distance X downstream of the interaction region becomes sufficiently large. This can be done (to a first approximation) by replacing the factor $\mathrm{e}^{\mathrm{i}\kappa X}$ by (Smith 1979)

$$\exp\left(\mathrm{i}\int_0^X \kappa\,\mathrm{d}X\right) = \exp\left(\frac{\mathrm{i}}{\epsilon^3}\int_0^x \kappa(x)\,\mathrm{d}x\right),$$

where the complex wavenumber κ is now to be evaluated at the local conditions. The absolute value of this factor determines the order of magnitude of the Tollmien–

Schlichting wave velocity fluctuation u_{TS} far (in terms of X) downstream from the interaction zone, since its coefficients are $O(1)$ in (4.9) and (4.10).

On the other hand, the analysis of Goldstein (1983*a*,*b*) and Goldstein *et al.* (1983) for the infinitely thin flat plate shows that the order of magnitude of u_{TS} is, in that case, determined by the factor

$$\epsilon^{-2\tau}\left|\exp\left(\frac{\mathrm{i}}{\epsilon^3}\int_{-1}^{x}\kappa\,\mathrm{d}x\right)\right| = \epsilon^{-2\tau}\left|\exp\left(\frac{\mathrm{i}}{\epsilon^3}\int_{-1}^{0}\kappa\,\mathrm{d}x\right)\right|\left|\exp\left(\frac{\mathrm{i}}{\epsilon^3}\int_{0}^{x}\kappa\,\mathrm{d}x\right)\right|,$$

where (Goldstein *et al.* 1983)

$$-2\tau \approx 1.3842$$

and we use the notation of the present paper. Notice that Goldstein's (1983*a*,*b*) ϵ and κ are respectively $S_0^{\frac{1}{8}}$ and $S_0^{-\frac{5}{8}}$ (evaluated at $x = 0$) times the present ϵ and κ. Thus the leading-edge Tollmien–Schlichting waves (on an infinitely thin flat plate) are weaker than those generated through the present mechanism by a factor of order

$$\epsilon^{1.384}\left|\exp\left(\frac{\mathrm{i}}{\epsilon^3}\int_{-1}^{0}\kappa\,\mathrm{d}x\right)\right|,$$

where $\epsilon^{1.384}$ is a measure of the strength of the coupling between the external disturbance and the Tollmien–Schlichting wave, i.e. it gives the order of magnitude of the coupling coefficient, and

$$\left|\exp\left(\frac{\mathrm{i}}{\epsilon^3}\int_{-1}^{0}\kappa\,\mathrm{d}x\right)\right|$$

is a measure of the damping that the wave undergoes before reaching the position $x = 0$, where the break point is located in the present study.

Assuming that the frequency parameter $\omega\nu/U_\infty^2$ is equal to Shapiro's (1977) value of 0.56×10^{-4} and using the estimate of the distance l to his break point given above, we infer from results given in Goldstein (1983*a*,*b*) that the damping factors†

$$\left|\exp\frac{\mathrm{i}}{\epsilon^3}\int_{0}^{x}\kappa\,\mathrm{d}x\right| \quad\text{and}\quad \left|\exp\frac{\mathrm{i}}{\epsilon^3}\int_{-1}^{x}\kappa\,\mathrm{d}x\right|$$

should be roughly 0.75×10^{-1} and 3×10^{-3} respectively at Shapiro's neutral-stability point.

Thus it would appear that the present mechanism produces Tollmien–Schlichting waves that have about $\frac{1}{10}$ of the amplitude of the imposed disturbance at the 'theoretical' neutral-stability point, while the edge-generated waves (on an infinitely thin flat plate) are only about 10^{-4} of the amplitude of that disturbance, which agrees roughly with Murdock's (1980) estimate. But the weak adverse pressure gradient between the break point and the neutral-stability point in Shapiro's experiment (see figure 4) must have reduced the Tollmien–Schlichting wave damping that actually occurred there. Since this gradient is $O(\epsilon^3)$, as can be seen from figure 4 and our estimate of ϵ, the resulting reduction in $\mathrm{Im}\,\kappa$ could also be $O(\epsilon^3)$, which would tend to make the damping factor

$$\left|\exp\frac{\mathrm{i}}{\epsilon^3}\int_{0}^{x}\kappa\,\mathrm{d}x\right|$$

much closer to unity than to our previous estimate of 10^{-1}.

† Goldstein's (1983*a*,*b*) $\tilde{x}_1$ corresponds to the parameter $S_0^{\frac{1}{8}}/\lambda^2$ used in the present paper, so that $\tilde{x}_1 \approx (0.73)^{\frac{1}{4}}/(0.332)^2 \approx 6$ at the neutral-stability point and $\tilde{x}_1 \approx 0.832$ at the break point.

This also implies that there was an upstream shift in the location of the neutral-stability curve in the Shapiro experiment (from its theoretical flat-plate value) which was, in fact, already suggested by Shapiro (1977). This is also supported by his data (see his figure 24), which show spatial growth of the measured instability wave in the region upstream of the theoretical neutral-stability curve.

5.2. *The numerical coefficient of the damping factor*

We now show that the numerical factor multiplying

$$\left| \exp \frac{\mathrm{i}}{\epsilon^3} \int_0^x \kappa \, \mathrm{d}x \right|$$

is, in fact, not too different from unity. The scaled skin-friction parameter λ is equal to 0.332... for a Blasius boundary layer, and we have inferred that $S_0 \approx 0.17$ in Shapiro's (1977) 29 m/s experiment. Then it follows from figure 2 of Goldstein† (1983*a*) and figure 5 of the present paper that $\eta \approx 1.44 \exp(-2.79\mathrm{i})$ and $|A(S_0/\lambda^{\frac{3}{2}})| \approx 0.36$. Using (5.2) for a discontinuous slope change across the interaction region to obtain an estimate of $h\bar{F}$, we find

$$h\bar{F} \approx 26.7 h\alpha_0 \, \mathrm{e}^{-0.52\mathrm{i}}.$$

We have already indicated that Shapiro (1977) measured the ratio of the maximum streamwise Tollmien–Schlichting wave velocity to that of the imposed disturbance, say $|u_{\mathrm{TS}}|_{\max}$, at the theoretical location of the lower branch of the neutral-stability curve in his experiment. Since

$$\lambda \frac{\displaystyle\int_\eta^{\eta+(1\mathrm{i}\lambda)^{\frac{1}{3}}Y} \mathrm{Ai}\,(\zeta)\,\mathrm{d}\zeta}{\displaystyle\int_\eta^{\infty} \mathrm{Ai}\,(\zeta)\,\mathrm{d}\zeta}$$

goes nearly monotonically to λ as $Y \to \infty$ and, since the maximum value of $U_{\mathrm{B}}'(y)$ is also λ, it follows from (4.9) and (4.10) that

$$|u_{\mathrm{TS}}|_{\max} \approx (h\alpha_0)\, 26.7\, (0.332)^2\, 0.36 \left| \exp\left(\frac{\mathrm{i}}{\epsilon^3}\int_0^x \kappa \, \mathrm{d}x\right)\right| \approx (h\alpha_0)\, 1.07 \left| \exp\left(\frac{\mathrm{i}}{\epsilon^3}\int_0^x k \, \mathrm{d}x\right)\right|.$$

Then in view of our previous argument that the last factor should be about unity in Shapiro's experiment, we infer that the ratio of the maximum neutral Tollmien–Schlichting wave to the imposed disturbance velocity should be about $1.07 h\alpha_0$ according to the present theory. This agrees with Shapiro's (1977) observation when $h\alpha_0 \equiv \alpha/\epsilon^2$ is about one, which, as was shown above, is consistent with his static pressure measurements.

5.3. *Application to small humps*

We have already indicated that the present analysis also applies to small humps or protuberances on otherwise-smooth walls. A typical protuberance shape function is

$$F(X) = \begin{cases} 1 & (-\frac{1}{2}d < X < \frac{1}{2}d), \\ 0 & (|X| > \frac{1}{2}d). \end{cases} \tag{5.3}$$

† See footnote on p. 524.

Then it follows from (3.26) that

$$\bar{F}(k) = \frac{\sin \frac{1}{2}kd}{k(\frac{1}{2}\pi)^{\frac{1}{2}}}. \tag{5.4}$$

Hence $\bar{F}$ and consequently the coupling coefficient (since Λ is independent of d, see (4.9)) will be a maximum, for fixed Tollmien–Schlichting wavenumber κ, when $\kappa d = \pi$, i.e. when d equals half the Tollmien–Schlichting wavelength $2\pi/\kappa$.

Aizin & Polyakov (1979) conducted a relevant experiment, whose results are published as an internal Russian report but are described in considerable detail by Nishioka & Morkovin (1985) (who also point out its connection with the present work). Their experiment is similar to Shapiro's (1977), but with the Tollmien–Schlichting wave generated by an upstream-propagating acoustic wave interacting with a thin Mylar strip affixed to the plate near the lower branch of the neutral-stability curve.

Such a strip is certainly well described by the shape function (5.3), and Nishioka & Morkovin (1984) indicate that the most efficient coupling occurred when the width d of the strip was equal to half the Tollmien–Schlichting wavelength, in agreement with the present theory, and that the coupling coefficient was equal to 1.39 times that produced by their basic $\frac{1}{4}$ wavelength strip, which is close to the factor $\sqrt{2}$ predicted by the present theory.

Aizin & Polyakov appear to have defined their coupling coefficient as the magnitude of the Tollmien–Schlichting wave amplitude divided by the magnitude of the Stokes shear-wave amplitude at the end of the Mylar strip and at some unspecified transverse distance from the wall. This should not be too different from the ratio of the maximum Tollmien–Schlichting wave amplitude to the maximum Stokes shear-wave amplitude – the latter being about $1.15u_\infty$ (Ackerberg & Phillips, 1972). Hence it follows from (4.9) and (5.4) that the appropriate coupling coefficient is

$$\frac{\lambda^2 hd}{1.15}\left|\frac{\sin \frac{1}{2}\kappa d}{\kappa d(\frac{1}{2}\pi)^{\frac{1}{2}}}\Lambda\left(\frac{S_0}{\lambda^{\frac{3}{2}}}\right)\right|, \tag{5.5}$$

which increases linearly with the scaled hump height h. This linear dependence is, as pointed out by Nishioka & Morkovin, well corroborated by the Aizin–Polyakov experiment.

It follows from (2.2) and (2.3) that (5.5) can be written as

$$\frac{\lambda^2 h^* d^*}{1.15\,(\frac{1}{2}\pi)^{\frac{1}{2}}}\left(\frac{R_{\delta^*}}{1.72l}\right)^2\left|\Lambda\left(\beta\left(\frac{R_{\delta^*}}{1.72\lambda}\right)^{\frac{3}{2}}\right)\frac{\sin \frac{1}{2}\kappa d}{\delta d}\right|, \tag{5.6}$$

where h^* and d^* denote the dimensional protuberance height and width respectively, $\beta \equiv \omega\nu/U_\infty^2$ is the frequency parameter and, as before, R_{δ^*} denotes the displacement-thickness Reynolds number.

The maximum coupling coefficient measured by Aizin & Polyakov was between 0.0034 and 0.0047. It corresponded to an average h^* of 0.0345 mm, $R_{\delta^*} = 1550$, $\beta = 25.4 \times 10^{-6}$, $l = 565$ mm and $d^* = 12$ mm, so that κ was nearly real and $d\kappa = \frac{1}{2}\pi$ in this case. Inserting these numbers into (5.6) and using figure 5, we find that $|\Lambda| \approx 1.05$, and consequently that the maximum coupling coefficient should be about 0.038, which is remarkably close to the observed value. Under the same conditions, but with an average h^* of 0.0225 mm, the computed coupling coefficient is 0.025, which is also close to the observed value of 0.025–0.028. It should be noted that Aizin & Polyakov made an equally good prediction based on an unclear feedback model, which appears to be completely unrelated to the present mechanism.

Equation (5.6) indicates that the coupling coefficient should vanish when $d\kappa = 2\pi$, as does the Aizin & Polyakov formula. For this case they measure a coupling coefficient of 0.006, which is close to the value they measured without the Mylar strip. They attribute this to the basic surface-geometry change at the junction between their nose and flat-plate regions, but it may also be due to the original leading-edge mechanism of Goldstein (1983*a*) and Goldstein *et al.* (1983).

5.4. *Extension to other disturbances*

Although the present work was, for definiteness, restricted to acoustic disturbances, it applies equally well to any imposed disturbance whose spatial scale is large compared with the Tollmien–Schlichting wavelength (i.e. to the size of the triple deck). It is only necessary to reinterpret the free-stream fluctuation amplitude u_∞, which multiplies the entire dimensional unsteady solution, as the, possibly complex, amplitude of the inviscid velocity fluctuation just outside the triple-deck (or interaction) region. The final results ((4.9) and (4.10)) therefore apply to convected disturbances, which can be superposed to represent free-stream turbulence, and to sufficiently long-wavelength plate vibrations. The latter application would, of course, involve an auxiliary inviscid linear calculation to relate the streamwise velocity fluctuation u_∞ to the prescribed plate displacement.

Since the theory is linear, the results can be superposed to deal with various combinations of imposed disturbances. In this regard it is worth mentioning a recent experiment of Gedney (1983), who used Shapiro's (1977) original apparatus with the acoustic speaker turned on and simultaneously vibrated the plate with a driving rod connected to its lower surface. The amplitude and phase of the plate vibration were adjusted until the speaker-generated Tollmien–Schlichting waves could no longer be detected. The implication of the present theory is that the net complex amplitude u_∞ (of the acoustic and plate vibration induced inviscid disturbance just outside the triple deck) was caused to vanish. In other words, it was the source of the Tollmien–Schlichting wave itself that was actually eliminated in this experiment.

5.5. *Extension to higher frequencies and smaller humps*†

This paper is concerned with high-Reynolds-number Blasius boundary layers for which the frequency parameter $\beta \equiv S/R = S_0\epsilon^6$ is proportional to $R^{-\frac{3}{4}}$ along the lower branch of the Tollmien–Schlichting wave neutral stability curve, and to $R^{-\frac{3}{5}}$ along its upper branch. We have already indicated that these waves have wavelengths $O(\epsilon^3)$ and consequently exhibit the well known triple-deck structure in the region $\beta = O(R^{-\frac{3}{4}})$ (i.e. in the region where $S_0 = O(1)$) lying below and in the viscinity of the lower branch, but the Bodonyi & Smith (1981) analysis shows that they exhibit a four-layer structure in the much larger unstable region, $\beta = O(R^{-\frac{3}{5}})$, lying between these curves, because $S_0 \gg 1$ and they have much shorter wavelengths $= O(\epsilon^3/\sqrt{S_0})$ there.

While the present analysis was restricted to the former region and specific results were only given for the case where the mean flow is linearizable about the Blasius flow, it turns out that the final formula, actually its high-frequency limit (4.15), applies to the entire unstable (and much larger) region where $\beta = O(R^{-\frac{3}{5}})$ – even when the mean flow cannot be linearized. This occurs because (1) the additional layer of Tollmien–Schlichting-wave structure is actually contained in the lower part of the main deck to the order of approximation of the present analysis (Bodonyi & Smith,

† Some of the material in this section is related to a recent study of Burggraf & Smith (1985).

1981), and (2) the resulting higher frequency Tollmien–Schlichting waves are now connected with a portion of the unsteady flow (i.e. the interactive portion associated with the upper deck motion) that depends only on the wall boundary conditions in the interaction region and not on the mean-flow variations produced by those conditions.

The streamwise lengthscale of the wall displacement in the interaction region must of course approach zero along with the Tollmien–Schlichting wavelength, i.e. it must scale with $\epsilon^3/\sqrt{S_0}$ as $S_0 \to \infty$, if these waves are still to be generated by the interaction. Fortunately, the steady flow over humps of such short lengthscales has already been analysed by Smith, Brighton, Jackson & Hunt (1981) and by Smith & Daniels (1981). They show that this flow is still described (in a certain restricted sense) by the triple deck and that it will separate when the hump height exceeds $O(\epsilon^5 S_0^{-\frac{1}{6}})$, which is the height where the mean-flow disturbance first becomes nonlinear in the viscinity of the hump. But (4.15) will apply even to much larger humps (of height $= O(\epsilon^5)$), which produce separation of the downstream flow, it we simply replace the scaled wall displacement F in the Fourier transform $\overline{F}$ by the scaled transverse position F_S of the separated streamline in the region of separated mean flow (since the separated streamline is too close to the wall to sustain any new instabilities). Of course F_S, and consequently the result (4.15), will then depend on the mean flow, which was discussed in part by Smith & Daniels (1981) and which in general can only be determined from the full nonlinear and viscous-triple-deck solution.

Its most interesting feature (from our point of view) is that the main portion of the lower deck becomes inviscid in the vicinity of the hump (i.e. where $X = O(S^{-\frac{1}{2}})$), with the viscous effects confined to a narrow wall layer in which the motion is governed by the boundary-layer equation with the pressure related to the streamwise velocity at infinity in the usual way. The streamwise velocity is equal to the scaled wall displacement hF when $h \ll 1$ in our notation, as was pointed out by Smith & Daniels (1981), but is related to the latter in a much more complicated way that depends on the upstream vorticity distribution when $h = O(1)$. The preicse relation can be found from the solution of the inviscid boundary-layer equation, which is easily obtained in closed form. Finally, it is worth noting that the vorticity in the separated region is not necessarily equal to zero and that the growth rate of the Tollmien–Schlichting wave will be affected by the mean flow in this region.

Since the form of the Fourier transform requires that $\overline{F}(\sqrt{\lambda S_0})$ be $O(S_0^{-\frac{1}{2}})$ and h cannot exceed $O(S_0^{-\frac{1}{6}})$ when the flow is unseparated, (4.15) implies that the coupling coefficient (between the Tollmien–Schlichting wave and the external disturbance) will be $O(S_0^{-\frac{1}{2}})$ when the flow is separated and $O(S_0^{-\frac{2}{3}})$ when it is not.

Bodonyi & Smith, (1981) showed that $S_0 = O(R^{\frac{3}{10}})$ near the upper branch of the neutral stability wave and it is easily shown that this scaling applies over most of the unstable region. It therefore follows that the coupling coefficient will be $O(R^{-\frac{3}{20}})$ there, when the flow is separated and $O(R^{-\frac{1}{10}})$ when it is not.

6. Concluding remarks

The order-of-magnitude analysis of §5 suggests that Shapiro's (1977) acoustic disturbance is coupled to the Tollmien–Schlichting waves via the small surface geometry variations in his experiment and not by the weak leading-edge coupling mechanism studied by Murdock (1980) and Goldstein (1983*a*). This does not, of course, mean that the latter mechanism will not be dominant in other experiments. In any case, it seems to us that the relevant physics of both mechanisms can only be put into perspective by a mutual comparison of the type given in §5.

I would like to thank Bruce Auer for carrying out the numerical computations and Professor M. V. Morkovin for his helpful comments and for bringing the Aizin–Polyakov experiment to my attention.

REFERENCES

ABRAMOWITZ, M. & STEGUN, I. A. 1964 *Handbook of Mathematical Functions.* National Bureau of Standards.

ACKERBERG, R. C. & PHILLIPS, J. H. 1972 *J. Fluid Mech.* **51**, 137.

AIZIN, L. B. & POLYAKOV, M. F. 1979 Acoustic generation of Tollmien–Schlichting waves over local unevenness of surface immersed in streams (in Russian). *Preprint* 17, *Akad. Nauk USSR, Siberian Div., Inst. Theor. Appl. Mech., Novosibirsk.*

BODONYI, R. J. & SMITH, F. T. 1981 *Proc. R. Soc. Lond.* A **375**, 65–92.

BOGDANOVA, E. V. & RYZHOV, O. S. 1983 *Q. J. Mech. Appl. Maths* **36**, 271.

BROWN, S. N. & DANIELS, P. G. 1975 *J. Fluid Mech.* **67**, 743.

BURGGRAF, O. R. & SMITH, F. T. 1985 On the development of large-sized short-scaled disturbances in boundary layers (leading to the Benjamin–Ono, KdV and Burger's equations). To be published in *Proc. R. Soc. Lond.* A.

GEDNEY, C. J. 1983 *Phys. Fluids* **26**, 1158.

GOLDSTEIN, M. E. 1981 *J. Fluid Mech.* **104**, 217.

GOLDSTEIN, M. E. 1983*a* *J. Fluid Mech.* **127**, 59.

GOLDSTEIN, M. E. 1983*b* Generation of Tollmien–Schlichting waves by free-stream disturbances at low Mach numbers. *NASA TM* 83026.

GOLDSTEIN, M. E. 1984 *J. Fluid Mech.* **145**, 71.

GOLDSTEIN, M. E., SOCKOL, P. M. & SANZ, J. 1983 *J. Fluid Mech.* **129**, 443.

HALL, P. & SMITH, F. 1982 *Stud. Appl. Maths* **66**, 000.

LEEHEY, P. & SHAPIRO, P. 1979 In *Laminar–Turbulent Transition* (ed. R. Eppler & H. Fasel), pp. 321–331. Springer.

LIN, C. C. 1946 *Q. Appl. Maths* **3**, 277.

MESSITER, A. F. 1970 *SIAM J. Appl. Maths* **18**, 241.

MURDOCK, J. W. 1980 *Proc. R. Soc. Lond.* A **372**, 517.

NAPOLITANS, WERLE, M. & DAVIS 1979 *AIAA J.* **17**, 000.

NISHIOKA, M. & MORKOVIN, M. V. 1985 Boundary-layer receptivity to unsteady pressure gradients: experiments and overview, submitted to *J. Fluid Mech.*

RAGAB & NAYFEH, A. 1980 *AIAA Paper* 80–0072.

REID, W. H. 1965 In *Basic Developments in Fluid Dynamics*, vol. I (ed. M. Holt), pp. 249–307. Academic.

SHAPIRO, P. J. 1977 The influence of sound upon laminar boundary layer instability. *MIT Acoustics and Vibration Lab. Rep.* 83458–83560–1.

SMITH, F. T. 1973 *J. Fluid Mech.* **57**, 803.

SMITH, F. T. 1979 *Proc. R. Soc. Lond.* A **366**, 91.

SMITH, F. T., BRIGHTON, P. W. M., JACKSON, P. W. & HUNT, J. C. R. 1981 *J. Fluid Mech.* **113**, 123–152.

SMITH, F. T. & DANIELS, P. G. 1981 *J. Fluid Mech.* **110**, 1–37.

STEWARTSON, K. 1969 *Mathematika* **16**, 106.

STEWARTSON, K. 1970 *Q. J. Mech. Appl. Maths* **23**, 137.

STEWARTSON, K. 1971 *Q. J. Mech. Appl. Maths* **24**, 387.

SYKES, R. I. 1978 *Proc. R. Soc. Lond.* A **361**, 225.

TAM, C. K. W. 1971 *J. Fluid Mech.* **46**, 757.